Journal of Solid State Chemistry **158,** 187–197 (2001)
doi:10.1006/jssc.2001.9092, available online at http://www.idealibrary.com on IDEAL®

Structural Characterization of $Li_{1-z-x}Ni_{1+z}O_2$ by Neutron Diffraction

C. Pouillerie,*,† E. Suard,‡ and C. Delmas*,[1]

*Institut de Chimie de la Matière Condensée de Bordeaux-CNRS and Ecole Nationale Supérieure de Chimie et Physique de Bordeaux, 87, Avenue Dr A. Schweitzer, 33608 Pessac cedex, France; †SAFT, Direction de la Recherche, 111 Bd. A. Daney, 33074 Bordeaux cedex, France; and ‡Institut Laue-Langevin, Avenue Jules Horowitz, BP 156, 38042 Grenoble cedex 9, France

Received August 7, 2000; in revised form January 3, 2001; accepted January 19, 2001

Pristine $Li_{1-z}Ni_{1+z}O_2$ ($z = 0.02$, 0.07, and 0.25) and deintercalated $Li_xNi_{1.02}O_2$ ($x = 0.82$ and 0.63) phases were characterized by neutron diffraction. In all cases, the amount of nickel in the lithium sites was found to be identical to that deduced from X-ray diffraction experiments. The sensitivity of the neutron studies allowed us to show that no lithium ions are in the NiO_2 slabs for $z = 0.02$ and 0.07. A Li/Ni mixing appears only for the most lithium-deficient phase leading to the $[Li_{0.73}Ni_{0.27}]_{3b}[Ni_{0.98}Li_{0.02}]_{3a}O_2$ cationic distribution for the $Li_{0.75}Ni_{1.25}O_2$ phase. Determination of the anisotropic atomic displacement parameters confirms the results previously obtained from EXAFS data. The structural characterization of partially deintercalated phases was in good agreement with the XRD analysis. However, in the case of $Li_{0.63}Ni_{1.02}O_2$, it gave evidence for the presence of a small amount of rhombohedral phase due to fluctuations in the composition of the starting material.

Key Words: **lithium nickelate; neutron diffraction; electrode materials; lithium batteries; intercalation.**

INTRODUCTION

The $Li_{1-z}Ni_{1+z}O_2$ series ($0 \le z \le 1$) were extensively studied in order to describe the evolution of the cationic distribution when lithium is progressively substituted for nickel (1–5). It is well known that a rhombohedral distortion of the cubic cell symmetry, observed for NiO, occurs for $z < 0.4$ due to the progressive ordering of the lithium and nickel ions into alternate (111) planes of the cubic cell (1, 6). For the ideal $LiNiO_2$ composition, the cationic distribution is expected to be perfectly ordered and the structure of the material can be described as a packing of NiO_2 slabs separated by lithium layers (Fig. 1). The 2D structural character of the $Li_{1-z}Ni_{1+z}O_2$ phases ($z \to 0$) allows one to use these materials as positive electrodes of lithium-ion batteries, since lithium ions can be reversibly intercalated and deintercalated within the structure (7–12).

[1] To whom correspondence should be addressed. E-mail: Delmas@icmcb.u-bordeaux.fr.

If, for strongly lithium-deficient $Li_{1-z}Ni_{1+z}O_2$ ($z \ge 0.20$) phases, it is generally agreed that a partial Li/Ni cation mixing occurs between the slabs and the interslab spaces, for materials closer to the ideal stoichiometry ($z \to 0$), some discrepancies remain to describe the distribution of the lithium and nickel ions within the structure. Indeed, two different structural hypotheses were previously assumed: either a cationic disorder only exits in the lithium layers resulting from the presence of the extra-nickel ions in the interslab spaces, or a cationic mixing occurs between the slabs and the interslab spaces implying the presence of lithium ions in the nickel layers and vice versa. One can think that these confusions are most likely linked to the use of X-ray diffraction for structural characterization (4, 5, 13–17). Indeed, Rietveld refinement of the X-ray diffraction patterns allows the determination, in a very accurate way, of the amount of extra-nickel ions present in the interslab spaces, but it does not allow the detection of a small amount of lithium ions in the nickel layers, due to the low scattering power of lithium compared to that of nickel.

As a result of the difference between the coherent scattering lengths of lithium and nickel ($b(Li) = -0.19\ 10^{-12}$ cm, $b(Ni) = 1.03\ 10^{-12}$ cm), neutron diffraction appears to be a powerful technique clarifying such structural details. Indeed, Reimers *et al.* (15) reported neutron diffraction study for a set of samples obtained in various synthesis conditions. For the best material, they found a cationic distribution close to $[Li_{0.97}Ni_{0.03}]_{3b}[Ni]_{3a}O_2$. Kanno *et al.* (13) reported a neutron diffraction study of a lithium nickel oxide very close to the ideal stoichiometry and found a small negative amount of Li in the $Ni_{(3b)}$ site. Therefore, they fixed the Ni occupancy in the slab to be unity. Pickering *et al.* (3) carried out a neutron diffraction analysis of high lithium-deficient $Li_{1-z}Ni_{1+z}O_2$ phases ($0.20 \le z \le 0.36$) and confirmed that when the departure from stoichiometry is large, a Li/Ni mixing exits between the slabs and the interslab spaces. Nevertheless, for intermediate departures from stoichiometry, one question remains opened: are there lithium ions in the nickel sites? This point is worth clarifying not only for the crystallographic point of view, but also for

0022-4596/01 $35.00

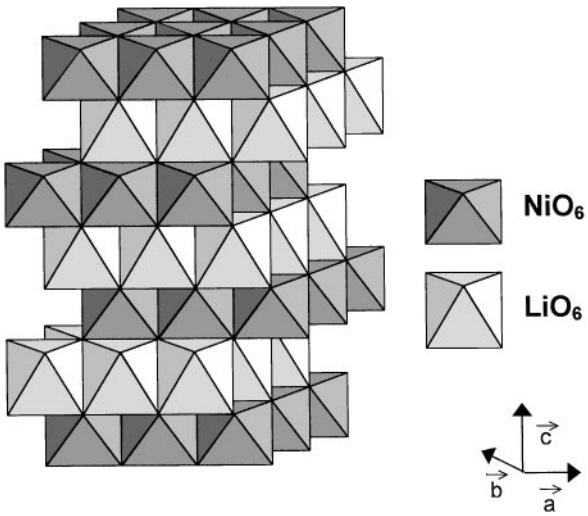

FIG. 1. Perspective view of the $LiNiO_2$ structure.

the application in lithium batteries. Indeed, if some Li^+ ions are present in the nickel layers, these ions will be removed during the deintercalation process, leading to the existence of vacancies in the nickel planes, which were recently shown to imply an increase of the a_{hex} cell parameter and to play an important role on the capacity stability upon cycling (18).

In this paper, we report the structural characterization by neutron diffraction of $Li_{1-z}Ni_{1+z}O_2$ phases with intermediate compositions ($z = 0.02, 0.07, 0.25$) in order to accurately determine their cationic distribution. In addition, we describe a detailed structural characterization by neutron diffraction of some deintercalated $Li_xNi_{1.02}O_2$ phases synthesized by electrochemical deintercalation from $Li_{0.98}Ni_{1.02}O_2$.

Previous characterizations by extended X-ray absorption fine structure (EXAFS) performed on two $Li_{1-z}Ni_{1+z}O_2$ phases ($z = 0.02$ and 0.10) showed the local distortion of the $Ni^{III}O_6$ octahedra due to the Jahn–Teller effect of the Ni^{3+} ions in the low spin state ($t_2^6e^1$) (17, 19–21). Due to the high quality of the neutron diffraction data, the anisotropic atomic displacement parameters can be determined for the oxygen and nickel ions, in the 6*c* and 3*a* sites, respectively, in order to describe the atomic displacements in the slabs and to confirm the EXAFS results. Therefore, in this paper, we report and discuss the results obtained for the anisotropic displacement parameters for both nickel and oxygen.

EXPERIMENTAL

Three lithium nickelate samples $Li_{1-z}Ni_{1+z}O_2$ ($z = 0$, 0.07, 0.25) were prepared by reacting a mixture of Li_2O and NiO. In all cases, an excess of lithium oxide (5%) was used in order to compensate for lithium loss during the calcination process. Powders were finely ground with a mortar and pestle within a dry box to form a homogeneous mixture, which was heated at 600°C for 10 h and at 700°C for 15 h under dry oxygen. An intermediate grinding was realized between the two high-temperature thermal treatments. The composition of the $LiNiO_2$ phase was previously determined by an X-ray analysis (22): 2% of extra-nickel ions were found in the interslab spaces. In this paper, this material will be designed by the formula deduced from the X-ray diffraction study: $Li_{0.98}Ni_{1.02}O_2$. The $Li_{0.82}Ni_{1.02}O_2$ and $Li_{0.63}Ni_{1.02}O_2$ delithiated phases were obtained by electrochemical lithium deintercalation from $Li_{0.98}Ni_{1.02}O_2$, following the electrochemical process described in (20).

Neutron diffraction data were recorded on the high-resolution powder diffractometer D2B of Institut Laue–Langevin (ILL), Grenoble (France) with the 1.593 Å wavelength. For $Li_{1-z}Ni_{1+z}O_2$ ($z = 0.02$, 0.07, and 0.25), the diffraction patterns were collected at ambient temperature from 0° to 162° (2θ) with a 0.05° step and a total counting time of 5 h. All the structures were determined by Rietveld refinement of the neutron diffraction patterns using the FULLPROF program (23).

RESULTS AND DISCUSSION

Neutron Diffraction Study of the Layered $Li_{1-z}Ni_{1+z}O_2$ Samples

Description of the Refinement Method

For all the structural refinements, a corrective term was used to take the sample absorption into account. The refinements were carried out assuming the layered $LiNiO_2$ structure in the space group $R\bar{3}m$. For the starting model, it was assumed that the 3*a* (0, 0, 0) site was only occupied by nickel ions, the 3*b* (0, 0, $\frac{1}{2}$) site by a mixture of Li and Ni ions in the ratio $(1 - z)/z$, and the 6*c* (0, 0, z_{ox}) site by O ($z_{ox} = 0.25$) (Fig. 1).

In a first step, the scale factor, cell parameters, zero shift, profile parameters, and position of oxygen z_{ox} were refined, constraining the isotropic atomic displacement parameter B_{iso} related to each site to be equal to 0.4 Å^2. This apparently quite arbitrary value results from our experience in neutron diffraction in these layered materials. It is only used in the beginning of the refinement and is afterward refined. Then, the amount z of extra-nickel ions present in the lithium site was precisely refined constraining the total occupancy of the 3*b* site to be equal to unity. In a third step, the degree of cationic disordering between the 3*a* and 3*b* sites was evaluated, allowing the exchange of a fraction (δ) of Li located in the 3*b* site for a fraction (δ) of Ni located in the 3*a* site. This leads to the occupancies

- for the 3*b* site: $(1 - z - \delta)$ Li and $(z + \delta)$ Ni,
- for the 3*a* site: $(1 - \delta)$ Ni and δ Li,

and therefore to the general cationic distribution

$$[Li_{1-z-\delta}Ni^{II}_{z+\delta}]_{3b}[Ni^{III}_{1-z}Ni^{II}_{z-\delta}Li_{\delta}]_{3a}O_2.$$

The starting exchange parameter δ was first assumed to be equal to zero (hypothesis of a perfect Li/Ni ordering) and then to be $(1 - z)/2$ (hypothesis of a total Li/Ni disordering) in order to check that the refinement leads to the same final value, whatever the starting hypothesis. At the fourth step, all parameters were simultaneously refined; in this case the isotropic atomic displacement parameters B_{iso} were independently refined for the 3*a*, 3*b*, and 6*c* sites. No divergence of the structural and profile parameters were observed in these refinements. Finally, anisotropic atomic displacement parameters were considered for the oxygen and nickel sites. The β_{ij} anisotropic coefficients were refined, taking into account the unit cell symmetry and their relation to the B_{iso} parameters. Then, the U_{ij} coefficient values, necessary to the description of the anisotropic atomic displacements around the crystallographic positions, were determined from the β_{ij} coefficients.

Structural Characterization

A Rietveld refinement of the neutron diffraction patterns collected at 300 K for $Li_{1-z}Ni_{1+z}O_2$ ($z = 0.02$, 0.07, and 0.25) was performed. For $Li_{0.93}Ni_{1.07}O_2$, the results of the refinement and the conditions of the data acquisition are given in detail in Tables 1 and 2. The main structural parameters and the cationic distribution are reported in Table 3 for the three phases. For $Li_{0.93}Ni_{1.07}O_2$, a comparison between the experimental and the calculated neutron diffraction patterns is given in Fig. 2: the small difference shows the good agreement achieved by the fit. For $Li_{0.98}Ni_{1.02}O_2$ and $Li_{0.75}Ni_{1.25}O_2$, the quality of the Rietveld refinements are very similar, as demonstrated by the small values obtained for the reliability factors (Table 3).

TABLE 1

$Li_{0.93}Ni_{1.07}O_2$		Constraints				
Space Group: *R*-3*m*		$n(Li_1) + n(Ni_1) = 1$				
$a_{hex} = 2.8803(2)$ Å		$n(Ni_2) + n(Li_2) = 1$				
$c_{hex} = 14.204(1)$ Å		$B(Li_1) = B(Ni_1)$ $B(Ni_2) = B(Li_2)$				
Atoms	Site	Wyckoff positions			B_{iso} (Å^2)	Occupancy
Li_1	3*b*	0.000	0.000	0.500	0.9(10)	0.93(1)
Ni_1	3*b*	0.000	0.000	0.500	0.9(10)	0.07(1)
Ni_2	3*a*	0.000	0.000	0.000	0.7(1)	1.00(1)
Li_2	3*a*	0.000	0.000	0.000	0.7(1)	0.00(1)
O	6*c*	0.000	0.000	0.2578(5)	1.1(2)	2.000
Conditions of the run						
Temperature		300 K				
Angular range		$0° \le 2\theta \le 162°$				
Step scan increment (2θ)		0.05°				
Zero point (2θ)		0.050(5)				
Number of fitted parameters		20				
Profile parameters						
Function profile: Pseudo-Voigt		$PV = \eta L + (1 - \eta)\ G$				
Eta		$\eta = 0.34(4)$				
Halfwidth parameters		$U = 0.12(1)$				
		$V = -0.16(3)$				
		$W = 0.17(1)$				

Note. Conventional Rietveld *R* factors for points with Bragg contribution: $R_{wp} = 12.4\%$; $R_B = 3.27\%$.

TABLE 2

Atoms	Site	U_{11}(Å^2)	U_{22}(Å^2)	U_{33}(Å^2)	U_{12}(Å^2)	U_{13}(Å^2)	U_{23}(Å^2)
Ni_2	3*a*	0.009(2)	0.009(2)	0.009(3)	0.004(2)	0	0
O	6*c*	0.017(4)	0.017(4)	0.007(3)	0.008(4)	0	0

Note. Conventional Rietveld *R* factors for points with Bragg contribution: $R_{wp} = 12.0\%$; $R_B = 3.17\%$.

Effect of the sample composition on the cationic distribution. In all cases, the compositions deduced from the Rietveld refinements are found to be in good agreement with the nominal formula. For $Li_{0.98}Ni_{1.02}O_2$, the neutron diffraction study leads to the same amount of nickel ions in the lithium sites as the amount deduced from previous X-ray diffraction analysis ($z = 0.02$) (22). No lithium ion is detected in the nickel sites for $Li_{0.98}Ni_{1.02}O_2$ and $Li_{0.93}Ni_{1.07}O_2$, since the δ exchange parameter is found to be equal to 0 in both cases. This study undoubtedly shows that slightly lithium-deficient $Li_{1-z}Ni_{1+z}O_2$ phases ($z \le 0.07$) do not exhibit any cationic mixing between the lithium and the nickel sites but only a statistical distribution of extra-nickel ions in the lithium sites. These results are in good agreement with the previous neutron diffraction studies realized by Kanno *et al.* on a quasi-2D lithium nickel oxide, for which no lithium ion was detected in the nickel sites (13).

In contrast, for $Li_{0.75}Ni_{1.25}O_2$, a very small Li/Ni mixing ($\delta \approx 0.02$) is observed between the lithium and the nickel sites. This result is in good agreement with the results reported by Pickering *et al.* on more strongly lithium-deficient $Li_{1-z}Ni_{1+z}O_2$ materials ($0.20 \le z \le 0.36$) (3). These authors found very weak Li/Ni mixings of about 1 and 4% for the $Li_{0.80}Ni_{1.20}O_2$ and $Li_{0.70}Ni_{1.30}O_2$ compositions respectively, while a significant amount of lithium ions (11%) was detected in the nickel layers for $Li_{0.64}Ni_{1.36}O_2$ (3). A neutron diffraction study of an $Li_{0.90}Ni_{1.10}O_2$ phase synthesized at 800°C in air for 3 h led Gummow and Thackeray (24) to propose the cationic distribution $[Li_{0.87}Ni_{0.13}]_{3b}[Ni_{0.97}Li_{0.03}]_{3a}O_2$. The degree of disordering in this compound is rather high compared to our results and those of Pickering *et al.* (3), but it shows that a larger Li/Ni mixing occurs when the thermal treatment is realized at higher temperature. Indeed, for an $Li_{0.76}Ni_{1.24}O_2$ composition prepared at 950°C in O_2, Rougier *et al.* (22) found from an X-ray diffraction study, the follow-

TABLE 3

Nominal formula	a_{hex}(Å)	c_{hex}(Å)	z_{ox}	z	δ	Cationic distribution	R_{wp}(%)	R_B(%)
$LiNiO_2$	2.8768(1)	14.1892(5)	0.2582(2)	0.022(4)	0.002(4)	$[Li_{0.98}Ni_{0.02}]_{3b}[Ni_1]_{3a}O_2$	10.2	2.74
$Li_{0.93}Ni_{1.07}O_2$	2.8803(2)	14.204(1)	0.2578(5)	0.07(1)	0.00(1)	$[Li_{0.93}Ni_{0.07}]_{3b}[Ni_1]_{3a}O_2$	12.0	3.17
$Li_{0.75}Ni_{1.25}O_2$	2.8958(1)	14.245(5)	0.2561(4)	0.250(5)	0.021(5)	$[Li_{0.73}Ni_{0.27}]_{3b}[Ni_{0.98}Li_{0.02}]_{3a}O_2$	12.4	2.75

ing cationic distribution: $[Li_{0.66}Ni_{0.34}]_{3b}[Ni_{0.90}Li_{0.10}]_{3a}O_2$. Therefore, comparison of our results with those of Gummow and Thackeray confirms that the preparation conditions and the history of the thermal treatments can strongly influence the composition and the cationic distribution of the lithium nickel oxides.

Evolution of the structural parameters with the sample composition. Figure 3 shows the variation of the hexagonal cell parameters and of the interatomic distances with the amount z of extra-nickel ions in the $Li_{1-z}Ni_{1+z}O_2$ phases ($z = 0.02$, 0.07, 0.25). The slab thickness $S_{(NiO_2)}$ and the interslab thickness $I_{(LiO_2)}$ are defined as $S_{(NiO_2)} = (2/3 - 2z_{ox})c_{hex}$ and $I_{(LiO_2)} = (c_{hex}/3) - S_{(NiO_2)}$. The data obtained by Pickering *et al.* (3) for $z = 0.20$, 0.306, 0.36 are also reported in Fig. 3.

As previously established, the existence of z extra-nickel ions in the lithium sites coupled with the lithium deficiency requires the presence of $2z$ Ni^{2+} ions and $(1 - z)$ Ni^{3+} ions in the structure. The steric considerations ($r_{Ni}^{3+} = 0.56$ Å, $r_{Ni}^{2+} = 0.69$ Å, $r_{Li+} = 0.74$ Å (25)) imply that divalent nickel ions are situated in the interslab spaces. These various points and the possible existence of an Li/Ni exchange between the 3*a* and 3*b* sites lead to the general cationic distribution for $Li_{1-z}Ni_{1+z}O_2$:

$$[Li_{1-z-\delta}Ni^{II}_{z+\delta}]_{3b}[Ni^{III}_{1-z}Ni^{II}_{z-\delta}Li_{\delta}]_{3a}O_2.$$

As shown in Table 3, $\delta < z$. Therefore, the above charge distribution can be considered likely.

The evolution of the structural parameters vs z is in good agreement with the results reported previously (3, 13, 22) and is strongly related to the cationic distribution of the materials described above. Indeed, from steric considerations, the presence of an increasing amount of divalent nickel ions within the NiO_2 slabs is responsible for the increase of the a_{hex} parameter (Ni–Ni intraslab distance), of the average Ni–O distance, and of the slab thickness $S_{(NiO_2)}$ when z increases. The same steric effects coupled with the strong electrostatic interactions between the divalent nickel cations and the oxygen ions explain the decrease of the average Li–O distance and of the $I_{(LiO_2)}$ interslab space thickness when the amount z of Ni^{2+} ions in the lithium sites increases. The increase with z of the c_{hex} distance shows

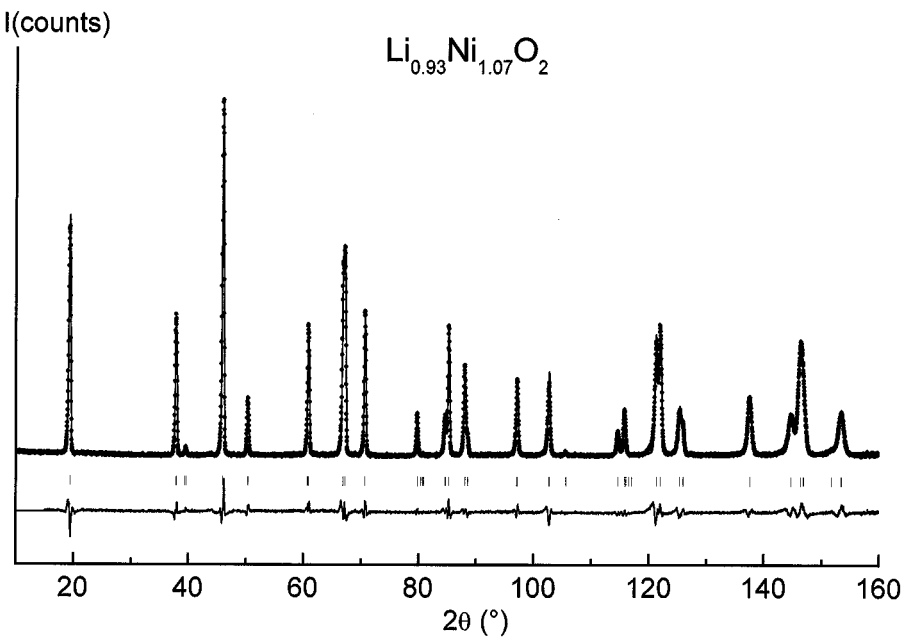

FIG. 2. Comparison of the experimental (—●—) ($\lambda = 1.593$ Å) and calculated (—) neutron diffraction patterns for $Li_{0.93}Ni_{1.07}O_2$; the difference between the experimental and the calculated patterns is also reported.

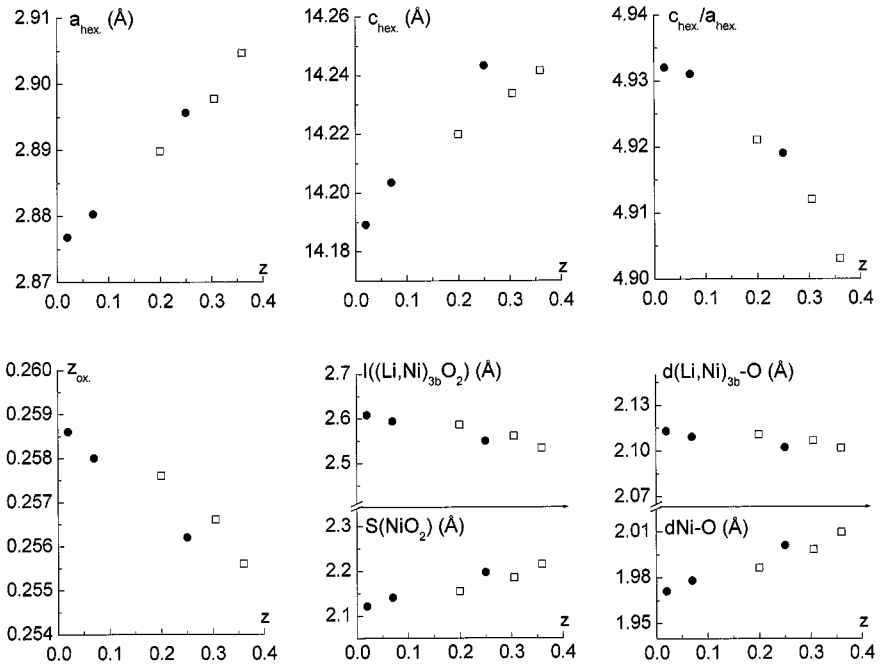

FIG. 3. Variation vs z of the cell parameters, the c/a ratio, the position of the oxygen atom (z_{ox}), the Ni–O and Li–O distances and of the slab and interslab thicknesses for the $Li_{1-z}Ni_{1+z}O_2$ phases: $z = 0.02$, 0.07, and 0.25 (●). The data for $z = 0.20$, 0.306, 0.36 (□) are taken from (3).

that the variation of the slab thickness is the prevailing effect.

A Li/Ni exchange between the 3*a* and 3*b* sites should tend to accentuate these evolutions, i.e., to shorten the average Li_{3b}–O distance and to lengthen the average Ni_{3a}–O distance. The increase of the $S_{(NiO_2)}$ slab thickness and the decrease of the $I_{(LiO_2)}$ interslab thickness with z (Fig. 3) lead to a decrease of the anisotropy of the structure, which therefore favors an Li/Ni exchange in the 3*b* and 3*a* sites when $z \geq 0.20$. Besides, the increasing Li/Ni mixing with z is consistent with the decrease of the z_{ox} and c/a values to 0.25 and 4.90, respectively, which are those obtained for a cubic symmetry characterized by a random Li/Ni distribution in the octahedral sites (Fig. 3).

Relation between the anisotropic oxygen displacement and the material composition. As shown for $Li_{0.93}Ni_{1.07}O_2$ in Table 2, the refinement of the neutron diffraction pattern, considering an anisotropic displacement of the nickel and oxygen atoms in the 3*a* and 6*c* sites, respectively, leads to a slight improvement of the refinement through a small decrease of the reliability factors. Table 4 gives the final U_{ij} anisotropic displacement parameters related to the Ni (3*a*) and O (6*c*) sites for the $Li_{1-z}Ni_{1+z}O_2$ phases ($z = 0.02$, 0.07, and 0.25). In the rhombohedral lattice mode of the trigonal symmetry, only the U_{11} and U_{33} parameters can be considered. The U_{11}(O) (respectively, U_{11}(Ni)) parameter describes the probability of displacement for the oxygen atoms (respectively, the nickel atoms) around their crystallographic position in the $(a, b)_{hex}$ plane parallel to the slab. The U_{33}(O) (respectively, U_{33}(Ni)) parameter corresponds to the probability of displacement of the atoms in the c_{hex} direction perpendicular to the slab. In Table 4, we have also specified the U_{11}/U_{33} ratio in order to describe the anisotropic character of atomic displacement in a more convenient way.

The results clearly show that the structure of the three lithium nickel oxides is characterized by:

— a quasi-isotropic displacement of the nickel ions, since $U_{11}(Ni)/U_{33}(Ni) = 1$ for $Li_{0.98}Ni_{1.02}O_2$ and $Li_{0.93}Ni_{1.07}O_2$ and is slightly smaller than 1 for $Li_{0.75}Ni_{1.25}O_2$,

— a preferential displacement of the oxygen ions in the $(a, b)_{hex}$ plane parallel to the slab rather than in the c_{hex} direction perpendicular to the slab, since $U_{11}(O)/U_{33}(O) > 1$ in all cases. In addition, the anisotropy of the oxygen displacement increases with the departure from stoichiometry z.

TABLE 4

Formula from Rietveld refinement	$Li_{0.98}Ni_{1.02}O_2$	$Li_{0.93}Ni_{1.07}O_2$	$Li_{0.75}Ni_{1.25}O_2$
U_{11}(Ni) (Å^2)	0.006(1)	0.009(2)	0.008(2)
U_{33}(Ni) (Å^2)	0.006(1)	0.009(3)	0.011(3)
U_{11}(O) (Å^2)	0.012(2)	0.017(4)	0.018(5)
U_{33}(O) (Å^2)	0.008(1)	0.007(3)	0.005(5)
U_{11}(Ni)/U_{33}(Ni)	1	1	0.73
U_{11}(O)/U_{33}(O)	1.5	2.43	3.6

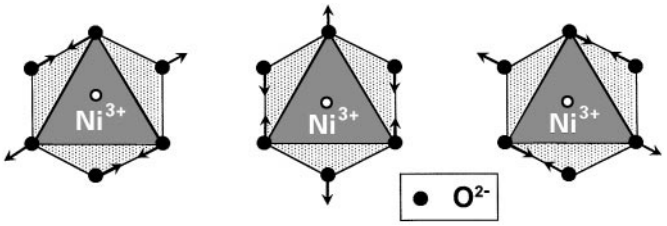

FIG. 4. Schematic representation of the oxygen displacements in the $(a, b)_{hex}$ plane parallel to the slab, due to the Jahn–Teller effect of the trivalent nickel ions in the low spin state $t_2^6e^1$. The oxygen motion occurs indifferently in the three equivalent directions of the triangular lattice.

An EXAFS study by Rougier *et al.* (17) on $Li_{0.98}Ni_{1.02}O_2$ gave evidence for the local distortion of the NiO_6 octahedra due to a noncooperative Jahn–Teller effect of the trivalent nickel ions in the low spin state $t_2^6e^1$, which entails the formation of two long Ni–O bonds (2.08 Å) and four short bonds (1.92 Å). In $NaNiO_2$, the Jahn–Teller effect leads to a cooperative monoclinic distortion resulting in the oxygen sheets gliding in the (a, b) plane. In the case of $Li_{0.98}Ni_{1.02}O_2$, due to the noncooperative character of the Jahn–Teller effect, this distortion occurs statistically along 3 equivalent directions in the (a, b) plane as shown in Fig. 4. Therefore, one can consider that the Jahn–Teller effect leads to an isotropic oxygen displacement in directions parallel with the slab planes. The results of the neutron diffraction study clearly confirm those of the EXAFS study for $Li_{0.98}Ni_{1.02}O_2$, since the observed anisotropic displacement of the oxygen ions must be related to the Jahn–Teller effect of the Ni^{III} ions. Note that this material is very close to the ideal stoichiometry, contrary to the other materials which are studied in the following.

A previous EXAFS study showed that, in the $Li_{0.90}Ni_{1.10}O_2$ phase, all the $Ni^{III}O_6$ octahedra are distorted since the localization of the divalent nickel ions of the slab in the vicinity of the divalent nickel ions of the interslab space, for charge compensation, prevents the existence of a significant hopping between the divalent and trivalent nickel ions, which would have inhibited the Jahn–Teller distortion of one part of the trivalent nickel ions (20). Moreover, the presence of a significant amount of divalent nickel ions in the slabs tends to distort locally the lattice, since the six oxygen anions which surround each Ni^{2+} ion are displaced from their ideal position, as shown in Fig. 5, leading to six long Ni–O bonds per Ni^{2+}. The effect of this local distortion on the neighboring $Ni^{III}O_6$ octahedra is difficult to analyze, but qualitatively the presence of an increasing amount of large-size divalent nickel ions tends to displace more and more the oxygen anions from the average position found in the structural refinement. Therefore, the higher values of the $U_{11}(O)/U_{33}(O)$ ratio found for $Li_{0.93}Ni_{1.07}O_2$ and $Li_{0.75}Ni_{1.25}O_2$ in comparison to the $Li_{0.98}Ni_{1.02}O_2$ ratio (Table 4) result from the additive contributions due to the Jahn–Teller effect and of the oxygen displacement around the divalent nickel ions. The value of the $U_{11}(Ni)/U_{33}(Ni)$ ratio smaller than 1 for the $Li_{0.75}Ni_{1.25}O_2$ phase shows that in this case, the nickel ions are preferentially displaced along the c_{hex} direction. One can assume that the presence of a large amount of Ni^{2+} ions in the lithium sites leads to local nickel ion displacements along this axis in order to accommodate the steric and electrostatic effects.

Neutron Diffraction Study of Deintercalated $Li_xNi_{1.02}O_2$ Phases ($x = 0.82, 0.63$)

Two delithiated $Li_{0.82}Ni_{1.02}O_2$ and $Li_{0.63}Ni_{1.02}O_2$ phases synthesized by electrochemical deintercalation from $Li_{0.98}Ni_{1.02}O_2$ were studied by neutron diffraction. The first phase exhibits a lithium composition close to the lower limit of the first rhombohedral solid solution, while the second phase corresponds to an intermediate composition of the monoclinic solid solution, which is observed in the wide $0.50 < x < 0.75$ composition range.

$Li_{0.82}Ni_{1.02}O_2$

The structure of $Li_{0.82}Ni_{1.02}O_2$ was refined in the $R\bar{3}m$ space group, using the structural model of the pristine material. The results of the refinement are given in Tables 5 and 6. Good agreement was obtained between the experimental and the calculated patterns, as shown in Fig. 6. The amount of extra-nickel ions in the lithium sites is the same as that of the starting phase. A decrease of the a_{hex} parameter and an increase of the c_{hex} parameter are observed upon lithium deintercalation as the result of the nickel ions oxidation and of the increase of the electrostatic repulsions between the slabs with the creation of lithium vacancies in the interslab space. The same steric and electrostatic effects explain the decrease of the $S_{(NiO_2)}$ slab thickness (from 2.123(6) Å to 2.074(9) Å) and the increase of the $I_{(LiO_2)}$ interslab thickness (from 2.606(6) Å to 2.672(9) Å) upon lithium

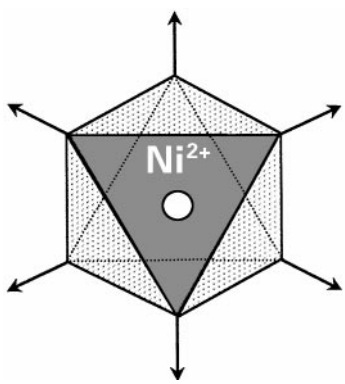

FIG. 5. Schematic representation of the oxygen displacements in the $(a, b)_{hex}$ plane parallel to the slab, due to the presence of one divalent nickel ion in the lattice mainly occupied by trivalent nickel ones.

TABLE 5

$Li_{0.82}Ni_{1.02}O_2$					Constraints	
Space Group: *R*-3*m*					$n(Li_1) = 0.82$	
$a_{hex} = 2.86696(8)$ Å					$n(Ni_1) + n(Ni_2) = 1.02$	
$c_{hex} = 14.2374(6)$ Å					$B(Li_1) = B(Ni_1)$	
Atoms	Site	Wyckoff positions			B_{iso} (Å^2)	Occupancy
Li_1	3*b*	0.000	0.000	0.500	0.9(4)	0.82
Ni_1	3*b*	0.000	0.000	0.500	0.9(4)	0.026(4)
Ni_2	3*a*	0.000	0.000	0.000	0.7(1)	0.994(4)
O	6*c*	0.000	0.000	0.2605(3)	1.1(1)	2.000

Conditions of the run	
Temperature	300 K
Angular range	$0° \le 2\theta \le 162°$
Step	0.05°
Zero point	0.050(5)
Number of fitted parameters	20
Profile parameters	
Function profile: Pseudo-Voigt	$PV = \eta L + (1 - \eta)\ G$
Eta	$\eta = 0.35(2)$
Halfwidth parameters	$U = 0.153(7)$
	$V = -0.19(2)$
	$W = 0.174(7)$

Note. Conventional Rietveld *R* factors for points with Bragg contribution: $R_{wp} = 8.92\%$; $R_B = 3.13\%$.

deintercalation from $Li_{0.98}Ni_{1.02}O_2$. Determination of the U_{ij} anisotropic displacement parameters (Table 6) gives evidence for a quasi-isotropic displacement of O (6*c*). The U_{11}(O) value is close to that of the parent compound

TABLE 6

Atoms	Site	U_{11}(Å^2)	U_{22}(Å^2)	U_{33}(Å^2)	U_{12}(Å^2)	U_{13}(Å^2)	U_{23}(Å^2)
Ni_2	3*a*	0.009(1)	0.009(1)	0.006(2)	0.005(1)	0	0
O	6*c*	0.014(2)	0.014(2)	0.013(3)	0.007(2)	0	0

Note. Conventional Rietveld *R* factors for points with Bragg contribution: $R_{wp} = 8.84\%$; $R_B = 2.91\%$.

$Li_{0.98}Ni_{1.02}O_2$, while the U_{33}(O), which is characteristic of atomic displacements perpendicular to the slab plane, has significantly increased. An EXAFS study showed the existence of short and long Ni–O bonds for this composition as in the $Li_{0.63}Ni_{1.02}O_2$ composition (26, 27). The *ex situ* study realized for the $Li_{0.63}Ni_{1.02}O_2$ composition shows that if almost all $Ni^{III}O_6$ octahedra are distorted at 77 K, only 70% of them are distorted at room temperature due to electronic hopping, which tends to kill the Jahn–Teller effect. To explain the apparent discrepancy between the neutron diffraction study and the EXAFS, one must consider the cationic distribution at the atomic scale. In deintercaleted materials, the lithium vacancies stay in the vicinity of the oxidized cations for charge compensation; therefore, in a layer structure there is a local tendency to decrease the slab thickness and to increase the interslab distance. This leads to local oxygen displacements perpendicular to the slab plane and, therefore, to an increase of the U_{33}(O) factor, which explains why a quasi-isotropic atomic displacement is observed for O (6*c*).

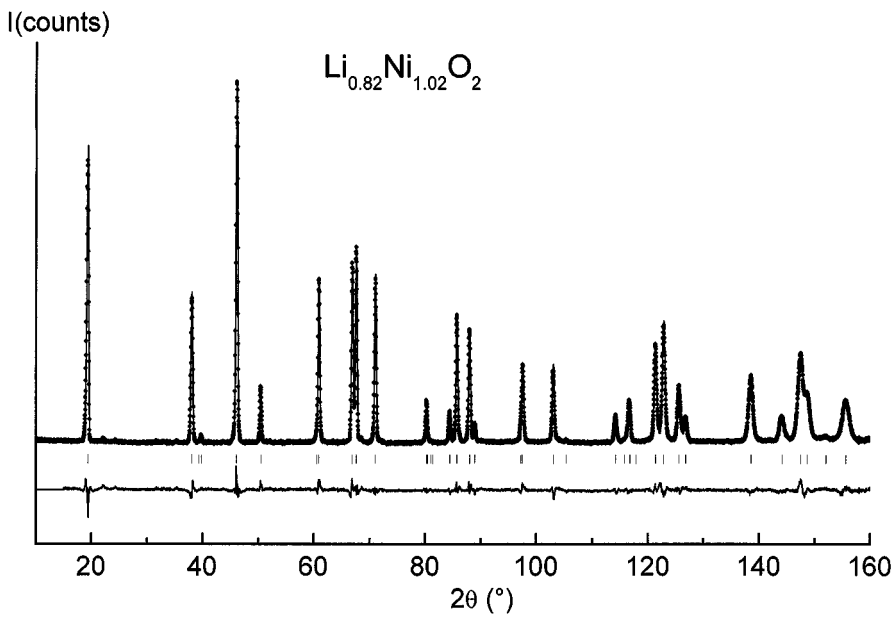

FIG. 6. Comparison of the experimental (—●—) ($\lambda = 1.593$ Å) and calculated (—) neutron diffraction patterns for $Li_{0.82}Ni_{1.02}O_2$; the difference between the experimental and the calculated patterns is also reported.

$Li_{0.63}Ni_{1.02}O_2$

$Li_{0.63}Ni_{1.02}O_2$ corresponds to an intermediate composition in the monoclinic solid solution. The structure of this phase was previously studied by Pérès *et al.* (20, 27) by X-ray diffraction, EXAFS, and electron diffraction. The latter study showed that the driving force of the monoclinic distortion is related to the existence of lithium/vacancy orderings which take place within the interslab spaces, due to a short-range in-plane repulsive interaction between lithium ions. Analysis of the neutron diffraction pattern of $Li_{0.63}Ni_{1.02}O_2$ does not show any additional diffraction line related to the superstructure cell observed by electron diffraction (27). This result was expected since simulations of the neutron diffraction pattern for ordered $Li_{0.63}Ni_{1.02}O_2$ lead to very weak intensity for the superstructure lines.

A Rietveld refinement of the neutron diffraction pattern was carried out in the C2/*m* monoclinic symmetry, with the structural parameters deduced from X-ray diffraction analysis (27). In this structural model, lithium and extra-nickel ions are located in the 2*d* $(0, \frac{1}{2}, \frac{1}{2})$ site, nickel in the 2*a* (0, 0, 0) site, and oxygen in the 4*i* (x_{ox}, 0, z_{ox}) site (with $x_{ox} \sim 0.25$ and $z_{ox} \sim 0.75$). The structure of the monoclinic phase is completely described with the determination of the oxygen atomic position, the occupancy parameters, and the thermal parameters. The structural parameters deduced from the refinement are given in Table 7. They are very similar to those deduced from the XRD study (27). Furthermore, the refinement leads to the same amount of extra-nickel ions in the lithium site as the pristine $Li_{0.98}Ni_{1.02}O_2$ phase. Satisfactory reliability factors are obtained with this structural hypothesis ($R_{wp} = 12.5\%$, $R_B = 4.70\%$) and relatively good agreement is observed between the experimental and the calculated patterns in Fig. 7. However, a careful comparison of the experimental and calculated patterns in some angular

TABLE 7

$Li_{0.63}Ni_{1.02}O_2$
Space Group: *C*2/*m*
$a_{mon} = 2.9894(5)$ Å
$b_{mon} = 2.8247(3)$ Å
$c_{mon} = 5.0656(6)$ Å
$\beta = 109.816(8)$ Å

Constraints
$n(Li_1) = 0.63$
$n(Ni_1) + n(Ni_2) = 1$
$B(Li_1) = B(Ni_1)$

Atoms	Site	Wyckoff positions			B_{iso} (Å^2)	Occupancy
Li_1	2*d*	0.000	0.500	0.500	1.0(10)	0.63
Ni_1	2*d*	0.000	0.500	0.500	1.0(10)	0.022(10)
Ni_2	2*a*	0.000	0.000	0.000	0.5(1)	0.998(10)
O	6*c*	0.734(1)	0.000	0.211(1)	0.9(2)	2.000

Conditions of the run	
Temperature	300 K
Angular range	$0^\circ \le 2\theta \le 162^\circ$
Step	0.05°
Zero point	0.050(5)
Number of fitted parameters	22
Profile parameters	
Function profile: Pseudo-Voigt	$PV = \eta L + (1 - \eta)\, G$
Eta	$\eta = 0.24(3)$
Halfwidth parameters	$U = 0.29(4)$
	$V = -0.17(3)$
	$W = 0.19(1)$

Note. Conventional Rietveld *R* factors for points with Bragg contribution: $R_{wp} = 11.2\%$; $R_B = 4.92\%$.

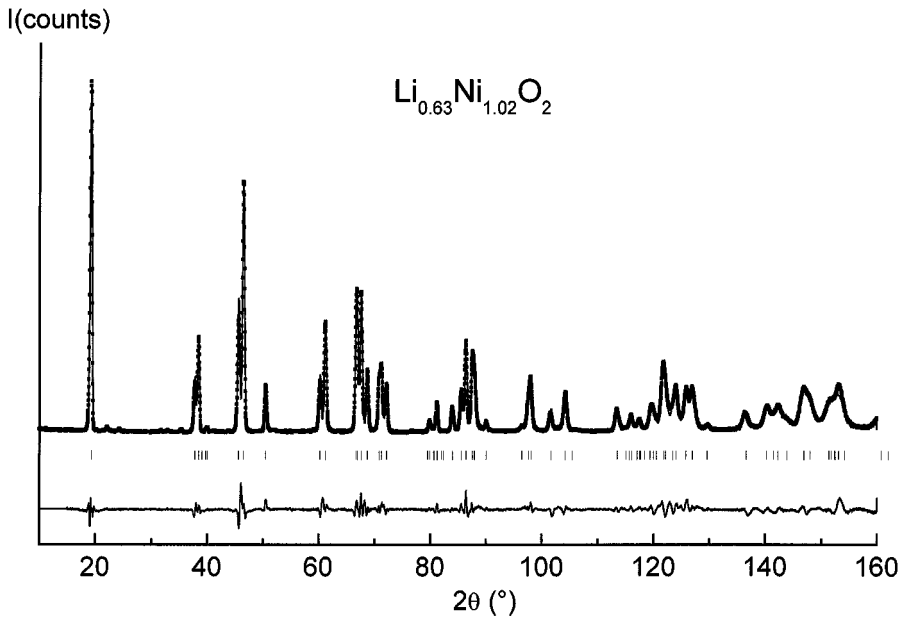

FIG. 7. Comparison of the experimental (—●—) ($\lambda = 1.593$ Å) and calculated (—) neutron diffraction patterns for $Li_{0.63}Ni_{1.02}O_2$; the difference between the experimental and the calculated patterns is also reported.

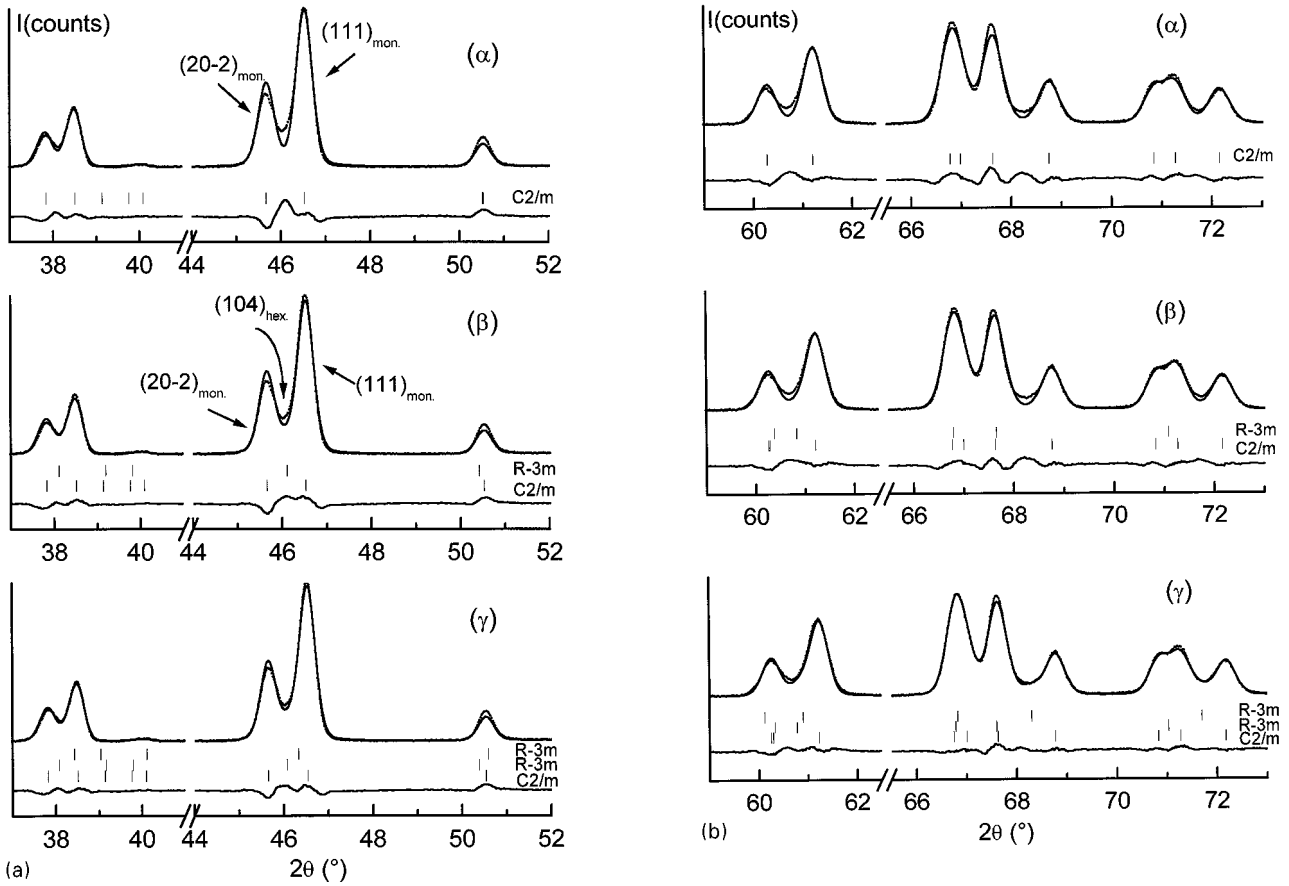

FIG. 8. Parts of the neutron diffraction pattern of $Li_{0.63}Ni_{1.02}O_2$ (—●—) in the (a) 37.5–52° (2θ) and (b) 59–73° (2θ) ranges ($\lambda = 1.593$ Å). The pattern was refined with the following structural hypotheses: one monoclinic phase ($C2/m$) (α); a mixture of one monoclinic phase and one rhombohedral phase ($R\bar{3}m$) (β); a mixture of one monoclinic phase and two rhombohedral phases ($R\bar{3}m$) (γ). The difference between the experimental (—●—) and the calculated (—) patterns is reported for each case. The bars corresponds to the position of the calculated diffraction lines related to the various phases.

domains shows that the structural model does not perfectly allow one to simulate the experimental pattern of $Li_{0.63}Ni_{1.02}O_2$. Indeed, a small discrepancy is in particular observed in the 37–52° and 59–73° (2θ) ranges (Fig. $8a_\alpha$ and $8b_\alpha$). In the former angular range, we can observe that the diffraction line shape does not only correspond to the superposition of the $(20\bar{2})_{mon}$ and $(111)_{mon}$ diffraction lines: the full pattern matching suggests the presence of at least one other diffraction line located in an intermediate position (28). This point was clearly found in our previous XRD studies of the monoclinic solid solution for several compositions ranging between $x = 0.50$ and 0.75, where a single phase was expected from the phase diagram. In all these experiments a shoulder was systematically found between the $(20\bar{2})_{mon}$ and $(111)_{mon}$ diffraction lines (29) and the full pattern matching gives evidence of at least one diffraction line located between these two monoclinic lines and attributed to a rhombohedral phase ($(104)_{hex}$). Note that the monoclinic distortion leads to a splitting of the $(104)_{hex}$ hexagonal line into the $(20\bar{2})_{mon}$ and $(111)_{mon}$ monoclinic lines. This result gives evidence for the nonhomogeneity of the $Li_{0.63}Ni_{1.02}O_2$ sample resulting from a nonhomogeneity of the starting intercalated material.

Rietveld refinement of the neutron diffraction pattern was performed again assuming that the studied sample consists of a mixture of the monoclinic phase and a small amount of one rhombohedral phase with close cell parameters. During this refinement, a small value was observed for the scale factor related to the rhombohedral phase, which means that no precise structural information could be reasonably deduced for this phase. Therefore, only its cell parameters were independently refined. The diffraction line shape vs the 2θ value was refined using the same pseudo-Voigt profile parameters and the same asymmetric parameters for the monoclinic and the rhombohedral phases. As shown in Fig. $8a_\beta$ and $8b_\beta$, a better agreement between the experimental and calculated patterns is observed with this structural hypothesis. This result is confirmed by the decrease of the R_{wp} reliability factor from 12.5 to 11.2%. Nevertheless, the refinement is not yet perfect. An improvement of the fit can

be obtained using two extra-rhombohedral phases (Fig. 8a$_\gamma$ and 8b$_\gamma$). In this case, the R_{wp} value is equal to 9.52%. The latter refinement does not allow one to determine the true phase composition of the sample but only gives evidence for its nonhomogeneity. One can expect that the material is probably constituted by a mixture of the monoclinic phase with a small amount of rhombohedral phases with very close compositions, which explains why the experimental pattern is not perfectly refined with the hypothesis of only one additional rhombohedral phase.

As previously suggested (28), this behavior is expected to be related to fluctuations in composition in the $Li_{0.98}Ni_{1.02}O_2$ starting material. Indeed, it is well known that the composition of the $Li_{1-z}Ni_{1+z}O_2$ phase is very sensitive to the experimental conditions. During the synthesis, there is a tendency to lose Li_2O, therefore one can assume that the composition is not exactly the same on the particle surface and in the bulk. Due to fluctuations in the distribution of the extra-nickel ions, the pristine material probably consists of a mixture of numerous phases with very close stoichiometries and very close structural parameters, which cannot be differentiated by the diffraction studies. When lithium deintercalation occurs, different structural behaviors are observed depending on the z value. The monoclinic solid solution domain is observed for the most part for the crystallites which are close to the ideal stoichiometry, while the crystallites with a larger amount of extra-nickel ions in the interslab space ($\geq 5\%$ (30)) do not exhibit the monoclinic distortion. This behavior explains why the problems of nonhomogeneity have not been evidenced for $Li_{0.82}Ni_{1.02}O_2$ but only for $Li_{0.63}Ni_{1.02}O_2$ by the neutron diffraction study. These results are in good agreement with those recently reported by (i) Croguennec *et al.* (31) who showed that the fluctuations in composition of the starting material also entail different structural behaviors, when almost all the lithium ions are removed from $LiNiO_2$, (ii) Reynaud *et al.* (32) who showed that the 240 K anomaly in the magnetic properties of some $LiNiO_2$ samples are due to the presence of macroscopic nickel-rich regions. This problem of nonhomogeneity in lithium nickel oxide will be the subject of a forthcoming paper.

CONCLUSION

The present neutron diffraction study shows that the cationic distribution of the $Li_{1-z}Ni_{1+z}O_2$ phases ($z = 0.02$ and 0.07) is characterized by the presence of z nickel ions in the lithium sites. There is no Li/Ni exchange between the slabs and the interslab spaces. For these compositions, the large Li^+ ions are destabilized in the small octahedral sites of the NiO_2 slabs. For materials with larger departure from stoichiometry, the presence of a larger amount of Ni^{2+} ions in the slabs and in the interslab spaces leads to a decrease of the interslab space distances and to an increase of the slab distances. The structure partially loses its anisotropy and a small Li/Ni mixing occurs. Due to the instability of lithium nickel oxide on the synthesis temperature, fluctuations in composition occur. Upon deintercalation, depending on the z value, a transition from the rhombohedral symmetry to the monoclinic symmetry can occur or not. The presence of a small amount of rhombohedral phases mixed with the monoclinic phase for the $Li_{0.63}Ni_{1.02}O_2$ composition emphasizes these fluctuations in stoichiometry.

ACKNOWLEDGMENTS

The authors thank J. P. Pérès for his active contribution and SAFT, CNES and Région Aquitaine, and ANRT for financial support.

REFERENCES

1. J. B. Goodenough, D. G. Wickahm, and W. J. Croft, *J. Appl. Phys.* **29**(3), 382 (1958).
2. L. D. Dyer, B. S. Borie, and G. P. Smith, *J. Am. Chem. Soc.* 1499 (1954).
3. I. J. Pickering, J. T. Lewandowski, A. J. Jacobson, and J. Goldstone, *Solid State Ionics* **405,** 53 (1992).
4. W. Li, J. N. Reimers, and J. R. Dahn, *Phys. Rev. B* **46,** 3236 (1992).
5. J. Morales, C. Pérez-Vicente, and J. L. Tirado, *Mater. Res. Bull.* **25,** 623 (1990).
6. W. Bronger, H. Bade, and W. Klemm, *Z. Anorg. Allg. Chem.* **333,** 188 (1964).
7. M. G. S. R. Thomas, W. I. F. David, J. B. Goodenough, and P. Groves, *Mater. Res. Bull.* **20,** 1137 (1985).
8. M. Broussely, F. Perton, J. Labat, R. J. Staniewicz, and A. Romero, *J. Power Sources* **43–44,** 209 (1993).
9. M. Broussely, F. Perton, P. Biensan, J. M. Bodet, J. Labat, A. Lecerf, C. Delmas, A. Rougier, and J. P. Pérès, *J. Power Sources* **54,** 109 (1995).
10. J. R. Dahn, U. Von Sacken, M. W. Juzkow, and H. Al-Janaby, *J. Electrochem. Soc.* **138**(8), 2207 (1991).
11. T. Ohzuku and A. Ueda, *Solid State Ionics* **69,** 201 (1994).
12. J. Farcy, J. P. Pereira-Ramos, L. Hernan, J. Morales, and J. L. Tirado, *Electrochim. Acta* **39**(3), 339 (1994).
13. R. Kanno, H. Kubo, Y. Kawamoto, T. Kamiyama, F. Izumi, Y. Takeda, and M. Takano, *J. Solid State Chem.* **110,** 216 (1994).
14. A. Hirano, R. Kanno, Y. Kawamoto, Y. Takeda, K. Yamaura, M. Takano, K. Ohyama, M. Ohashi, and Y. Yamaguchi, *Solid State Ionics* **78,** 123 (1995).
15. J. N. Reimers, J. R. Dahn, J. E. Greedan, C. V. Stager, G. Liu, I. Davidson, and U. Von Sacken, *J. Solid State Chem.* **102,** 542 (1993).
16. H. Arai, S. Okada, Y. Sakurai, and J. I. Yamaki, *Solid State Ionics* **95,** 275 (1997).
17. A. Rougier, C. Delmas, and A. V. Chadwick, *Solid State Comm.* **94**(2), 123 (1995).
18. C. Pouillerie, F. Perton, P. Biensan, J. P. Pérès, M. Broussely, and C. Delmas, *J. Power Sources*, in press.
19. I. Nakai, K. Takahashi, Y. Shiraishi, T. Nakagome, F. Izumi, Y. Ishii, F. Nishikawa, and T. Konishi, *J. Power Sources* **68**(2), 536 (1997).
20. J. P. Pérès, A. Demourgues, and C. Delmas, *Solid State Ionics* **111,** 135 (1998).
21. A. N. Mansour, J. McBreen, and C. A. Melendres, *J. Electrochem. Soc.* **146**(8), 2799 (1999).
22. A. Rougier, P. Gravereau, and C. Delmas, *J. Electrochem. Soc.* **143**(4), 1168 (1996).

23. J. Rodriguez-Carvajal, *in* "Satellite Meeting on Powder Diffraction of the XV Congress of the IUCr," p. 127, 1990.
24. R. J. Gummow and M. M. Thackeray, *Solid State Ionics* **53–56,** 681 (1992).
25. R. D. Shannon and C. T. Prewitt, *Acta Crystallogr*., *Sect*. *B*: *Struct*. *Sci*. **25,** 925 (1969).
26. A. N. Mansour, X. Q. Yang, X. Sun, J. McBreen, C. Delmas, and L. Croguennec, *in* "195th Meeting of the Electrochemical Society," 1999.
27. J. P. Pérès, F. Weill, and C. Delmas, *Solid State Ionics* **116**(1–2), 19 (1999).
28. C. Delmas, M. Ménétrier, L. Croguennec, S. Levasseur, J. P. Pérès, C. Pouillerie, G. Prado, L. Fournès, and F. Weill, *Int*. *J*. *Inorg*. *Mater*. **1,** 11 (1999).
29. J. P. Pérès, thesis, University of Bordeaux I, 1996.
30. A. Hirano, R. Kanno, Y. Kawamoto, K. Oikawa, T. Kamiyama, and F. Izumi, *Solid State Ionics* **86–88,** 791 (1996).
31. L. Croguennec, C. Pouillerie, and C. Delmas, *J*. *Electrochem*. *Soc*. **147**(4), 1314 (2000).
32. F. Reynaud, A. M. Ghorayeb, Y. Ksari, N. Menguy, A. Stepanov, and C. Delmas, *Eur*. *Phys*. *J*. *B* **14,** 83 (2000).